

ACCEPTED MANUSCRIPT

System Size Dependence of Final State Hadron Sources at Elab = 3.7A GeV

To cite this article before publication: A Abdelsalam *et al* 2019 *J. Phys. G: Nucl. Part. Phys.* in press <https://doi.org/10.1088/1361-6471/ab5d92>

Manuscript version: Accepted Manuscript

Accepted Manuscript is “the version of the article accepted for publication including all changes made as a result of the peer review process, and which may also include the addition to the article by IOP Publishing of a header, an article ID, a cover sheet and/or an ‘Accepted Manuscript’ watermark, but excluding any other editing, typesetting or other changes made by IOP Publishing and/or its licensors”

This Accepted Manuscript is © 2019 IOP Publishing Ltd.

During the embargo period (the 12 month period from the publication of the Version of Record of this article), the Accepted Manuscript is fully protected by copyright and cannot be reused or reposted elsewhere.

As the Version of Record of this article is going to be / has been published on a subscription basis, this Accepted Manuscript is available for reuse under a CC BY-NC-ND 3.0 licence after the 12 month embargo period.

After the embargo period, everyone is permitted to use copy and redistribute this article for non-commercial purposes only, provided that they adhere to all the terms of the licence <https://creativecommons.org/licenses/by-nc-nd/3.0>

Although reasonable endeavours have been taken to obtain all necessary permissions from third parties to include their copyrighted content within this article, their full citation and copyright line may not be present in this Accepted Manuscript version. Before using any content from this article, please refer to the Version of Record on IOPscience once published for full citation and copyright details, as permissions will likely be required. All third party content is fully copyright protected, unless specifically stated otherwise in the figure caption in the Version of Record.

View the [article online](#) for updates and enhancements.

System Size Dependence of Final State Hadron Sources at $E_{\text{lab}} = 3.7\text{A GeV}$

A. Abdelsalam^{1*}, M. S. El-Nagdy^{2*}, B. M. Badawy^{3*1}, and A. Saber^{4*}

¹Physics Department, Faculty of Science, Cairo University, Giza, Egypt.

²Physics Department, Faculty of Science, Helwan University, Helwan, Egypt.

³Reactor Physics Department, Nuclear Research Center, Atomic Energy Authority, Egypt.

⁴Department of Mathematical and Physical Engineering, Faculty of Engineering, Benha University, Shoubra, Egypt.

*Mohammad El-Nadi High Energy Lab, Faculty of Science, Cairo University, Egypt.

¹Email: he_cairo@yahoo.com

Abstract

3.7A GeV ^4He , ^{16}O , and ^{32}S beams from Dubna Synchrophasotron interacting in nuclear emulsion are used. The final state hadrons are approached by the produced shower particles. The dependence on the system size is examined. The data are discriminated according to the emission in the forward and backward zones over the 4π space. Minimum biased samples of events corresponding to average impact parameters are selected randomly. The data are compared to a simulation based on the modified FRITIOF event generator, implementing the Lund model string dynamics. The multiplicity characteristics present an overview of the parameters obtained when the distributions are fitted by the multisource thermal model. The forward emitted shower particles are suggested to be created in hadronization system due to multisource superposition. The backward emitted ones mostly result from target nucleus decay source in the framework of the limiting fragmentation hypothesis. Empirical parameterizations based primarily on fitting procedures are undertaken to fulfill the universality of some uniform relationships. Systematic uncertainties are estimated in terms of standard deviation within errors.

Key Words: Pion sources/ Modified FRITIOF model/ Multisource thermal model/ Collision system size.

PACS: 25.75.-q, 25.75.Dw, 25.75.Gz, 25.75.Ld, 25.70.Mn, 25.70.Pq, 41.75.Ak, 41.75.Cn, 29.40.Rg, 07.68.+m

1. Introduction

In the center of mass (CM) frame of the high-energy nuclear collision, the relative motion of the target nucleon versus projectile nucleon is slowed down because the energy is lost through the binary nucleon-nucleon (NN) collisions from the longitudinal to transverse degrees of freedom [1]. The energy is mainly transformed into newly created particles. In p+p collisions at ISR energies, the pionization components were referred to the final states [2]. Most of particles produced at the final states were pions [2, 3]. At Bevalac energies ($E_{\text{lab}} \sim 0.1A$ up to $2A$ GeV) [1], it was suggested that the energy is dissipated in internal excitation of the nucleon to produce baryon resonance and pions. In the framework of the statistical thermal model for high energy nuclear collisions [4], the final state hadron could result from strong decay, weak decay, or primarily production. At lower collision energies, the strong production of pions was mainly from Δ resonance. The decay of the short lived mesons (η and ρ) into pions became significant with increasing energy. The components of pions produced due to strong decay showed increase with the energy and tended to saturation at $\sqrt{s_{NN}} = 10$ GeV [4]. The main channels of the pion production in the weak decay were due to K_S^0 , Λ , $\bar{\Lambda}$, Σ^+ , $\bar{\Sigma}^-$, and Σ^- . The fraction of the pions produced in the weak decay reached the saturation at $\sqrt{s_{NN}} = 8$ GeV [4]. The results of the strong decay were in consistent with the

1
2
3
4
5
6 data from AGS, SPS, and RHIC [4]. The fraction of the primary production for final hadrons decreased
7 with increasing collision energy and somehow saturated near $\sqrt{s_{NN}} = 10$ GeV [4]. At lower energy, most
8 of the hadrons were from primary production, while the decay components would dominate at higher
9 energies [4]. The saturation of the primary production fraction indicated the limitation of the chemical
10 freeze-out temperature in hadronic interactions [4]. The position of the saturation for some hadrons
11 deviated from $\sqrt{s_{NN}} = 10$ GeV due to the contribution of quarks that are present in the colliding particles
12 or (target and projectile) [4]. The Lund string FRITIOF model [5, 6] assumed that the final state hadron
13 results from a resonance in a few GeV regions. Beyond the onset of the ultrarelativistic energies it
14 assumed that a quantum chromo dynamic (QCD) string is the source. In the framework of the quark-
15 gluon string model (QGS) [7] the considered energy ($\sqrt{s_{NN}} = 3.14$ GeV) was too small to produce
16 string masses. The dominant sources of pion at Dubna energies were resonance decay (Δ , ρ , ω , η , η') and
17 direct reactions [7].

18 The low nuclear matter densities can exist in the peripheral collision or in the low system size. In this
19 state a small part of energy is involved. The higher density fireball can be created in the central collisions
20 of heavy nuclei where higher energies are participated. In this state thermal and chemical equilibrium
21 properties are approached through sequences of binary NN collisions [8, 9]. The fireball of nuclear matter
22 or hadronic matter is formed in the participant nuclear matter, which is the origin of the creation sources.
23 In the rest frame of target, the energy is participated by the projectile nucleus. Kinematically, the created
24 pion is emitted in the forward hemisphere (FHS) at $\theta_{lab} < 90^\circ$. At Bevalac energies the fireball temperature
25 had a range from 30 up to 125 MeV [1]. This range is less than Hagedorn temperature of the hadronic
26 matter ~ 160 MeV. At average impact parameters of 3.7A GeV ^{12}C , ^{28}Si , and ^{32}S interactions with
27 emulsion nuclei [10] the temperature of the system producing forward emitted pion was predicted by
28 Hagedorn spectrum as ~ 112 MeV. This confirms that the forward emitted pion results from a fireball of
29 nuclear matter. The emission in the backward hemisphere (BHS) is restricted. Pion emission beyond the
30 kinematic limits at $\theta_{lab} \geq 90^\circ$ was suggested to be due to target fragmentation system, regarding the
31 limiting fragmentation hypothesis [11–15]. This was investigated and confirmed by our lab group [10,
32 16–20]. Two mechanisms were suggested to be responsible for this production. One is the nuclear cluster
33 decay in the cumulative region [21–24]. Since this pion results from a decay system, the emission is
34 possible at any direction in the 4π space. The other one was based on the effective target model [25, 26].
35 In that model the pion could be emitted at any direction in the 4π space due to its production from a single
36 NN scattering. The dominance of the latter mechanism existed in peripheral collisions or at $E_{lab} \leq 3$ GeV.
37 Bogatskaya et al [24] presumed that any particle production system has to be associated with a fireball.
38 Different fireballs are formed as gluonic fireball, quark fireball, baryonic fireball,-----etc. The different
39 fireballs have different velocities and temperatures. Hence, the backward emitted pion production source
40 also is expected to be associated with a fireball, which is completely different from that of the particle
41 creation.

42 The pion source varies according to the energy, system size, centrality, and emission zone. Our lab
43 group has concerned it [10, 16–20, 27–36]. The present interactions are 3.7A GeV ^4He , ^{16}O , and ^{32}S with
44 emulsion nuclei. This energy is the onset of the nuclear limiting fragmentation validity. This type of
45 experiments does not need a big amount of energy as that used with the collider ones to study the nuclear
46 fragmentation. Not only it can be guidelines in simulating and equipping the nuclear fragmentation
47 experiments but also in the modeling of some collider experiments. In the present experiment the
48 produced shower particle multiplicity is interested as a tool to investigate the final state hadron
49 production. The projectile size effect is examined over a qualitative wide range ($A_{proj} = 4, 16, 32$). Nuclear
50 emulsion usage can give a considerable wide range of target size ($A_T = 1$ up to 108). The produced
51 shower particles are classified according to their emission zone in the FHS and BHS. The data samples
52 are unbiased to any centrality criterion where they are selected randomly at average impact parameter.
53 The Monte Carlo simulation code used in this work is the modified FRITIOF model (MFM) [37–41]. The
54 multiplicity characteristics of the final-state hadrons are described in the framework of the multisource
55 thermal model (MTM) [42, 43], where the number of sources can be expected.
56
57
58
59
60

2. Models

2.1. Basic Concept of Modified FRITIOF Model (MFM)

The Lund string model [5] was used in the Monte Carlo events generator FRITIOF model [6]. The FRITIOF model could analyze the hadron–hadron (hh), hadron–nucleus (hA), and nucleus–nucleus (AA) interactions at high energy [6, 37, 44, 45]. In the model concept, the particle can be produced on the basis of the binary NN collisions. In the few GeV region (say Dubna energies) the collision results in resonance as; $NN \rightarrow N\Delta$. After a certain time, the meson is produced due to the resonance decay. In ultrarelativistic region (say SPS energies) the final state hadron can be produced through a continuum spectrum of an excited hadron. The hadron is considered a QCD string. If the mass of the excited string is less than a critical value (say 1.2 GeV for nucleon) it is considered a nucleon. The assumed interactions for the excited hadron production are $h_1 h_2 \rightarrow h_1^* h_2^*$ or $h_1 h_2 \rightarrow h_1 h_2^*$, where h_1^* and h_2^* are the hadron excited states. The 1st reaction is called non–diffractive interaction and the other is referred to single diffraction dissociation. Sampling the string mass is the base of the model, where the ground state mass of the hadron is the threshold. As a rule in the FRITIOF model, the Glauber–like approximation provides an insufficient amount of intranuclear cascading. The secondary particle cascading is neglected (It is known that the intranuclear cascading is an essential mechanism in the target multifragmentation system). Moreover, the resonance de–excitation, which is the source of the final–state hadron in a few GeV region, is neglected. As a result, the model failed to predict the nuclear destruction [37]. The model also was unsuccessful to predict the hadron multiplicity at $E_{\text{lab}} \leq 10A$ GeV [37] and hadron emission at large angles ($\theta_{\text{lab}} \geq 90^\circ$). The Reggeon theory was introduced to solve the problems by coupling the FRITIOF model with the binary cascade model, the so–called modified FRITIOF model [37–41, 45]. The enhanced diagrams of the Reggeon theory were illustrated in Ref. [39, 40], which amount the intranuclear cascading in the 2–dimensional space of the impact parameter. This modification could improve the results within 3.1A to 3.5A GeV. The present code modification was carried out by V. V. Uzhinskii, LIT, JINR, Dubna, Russia [38–40]. The code is based on the original FRITIOF version 1.6 [6, 44]. The input code parameters are obtained from Glauber's approach, which can be run by DIAGEN Monte Carlo generator events [46].

2.2. Basic Concept of Multisource Thermal Model (MTM)

This model [42, 43, 47] was introduced to describe the particle production in different collisions by uniform consideration. It is based on multisource ideal gas model [48–50]. It does not predict multisource in a single collision. It just statistically tries to fit data over a wide range of impact parameter, which defines rapidity. It also does not assign what the source is. The source contributes multiplicity distribution like a radioactive object. For a certain sample of events, let l groups of sources are contributed. The l groups consist of subgroups of sources, denoted j . Each subgroup consists of n_j of sources, m_j . The multiplicity distribution contributed by one source in the j^{th} subgroup is determined by Eq. (1), where $1 \leq i \leq m_j$ and i is natural number.

$$P_{ij}(n_{ij}) = \frac{1}{\langle n_{ij} \rangle} \exp\left(\frac{-n_{ij}}{\langle n_{ij} \rangle}\right) \quad (1)$$

$$\langle n_{ij} \rangle = \int n_{ij} P_{ij}(n_{ij}) dn_{ij} \quad (2)$$

where $\langle n_{ij} \rangle$ is the average multiplicity contributed by the i^{th} source in the j^{th} subgroup. It is assumed that $\langle n_{1j} \rangle = \langle n_{2j} \rangle = \dots = \langle n_{m_j j} \rangle$ (3)

The multiplicity distribution of one subgroup (j) contributed by m_j sources is determined by Erlang distribution Eq. (4). It is the fold of m_j exponential function.

$$P_j(n_{ch}) = \frac{n_{ch}^{m_j-1}}{(m_j-1)! \langle n_{ij} \rangle^{m_j}} \exp\left(\frac{-n_{ch}}{\langle n_{ij} \rangle}\right) \quad (4)$$

The average charged particle multiplicity $\langle n_{ch} \rangle$ in the j^{th} subgroup is determined by Eq. (5).

$$\langle n_{ch} \rangle = m_j \langle n_{ij} \rangle \quad (5)$$

The total multiplicity distribution contributed by l groups is determined by Eq. (6).

$$P(n_{ch}) = \sum_{j=1}^l k_j P_j(n_{ch}) \quad (6)$$

where k_j is the weight factor of the j^{th} subgroup. If the total multiplicity distribution is normalized to unity then, $\sum_{j=1}^l k_j = 1$. The average charged particle multiplicity $\langle n_{ch} \rangle$ is determined by Eq. (7).

$$\langle n_{ch} \rangle = \sum_{j=1}^l k_j m_j \langle n_{ij} \rangle \quad (7)$$

For e^+e^- , pp , $p\bar{p}$, and e^+p collisions $l = 1$. At very high energies $l = 2$ or 3 . For pA and AA collisions at fixed impact parameter, m_j can be regarded as the no of participant nucleon. The total distribution Eq. (5) is approximated statistically, where k_j , $\langle n_{ij} \rangle$, and m_j are obtained as fitting parameters.

3. Experimental Details

3.1. Photographic Nuclear Emulsion Detector and Target

The data under consideration are measured in nuclear emulsion which is used as a target. In the present experiment, 3 stacks of NIKFI-BR2 emulsion were irradiated by 3.7A GeV ^4He , ^{16}O , and ^{32}S at the Synchrophasotron, JINR, Dubna, Russia. The development of the emulsion stacks resulted in a shrinkage factor of about 2.2. The sensitivity of the plates is examined by measuring the grain density of the minimum ionizing particle track. It is found almost 28 grains per 100 μm on average. The dimensions of each pellicle in the stack are 20 cm \times 10 cm \times 0.06 cm. The atomic density (ρ) of each emulsion element is listed in Table (1). The experimental method and technique were detailed in previous publications [18, 51] of our lab.

Table (1): Elemental atomic density of the NIKFI-BR2 emulsion.

Element	^1H	^{12}C	^{14}N	^{16}O	^{80}Br	^{108}Ag
$\rho \times 10^{22} \text{ cm}^{-3}$	3.150	1.410	0.395	0.956	1.028	1.028

The charged particles tracks can be identified in the photographic nuclear emulsion according to the common terminology [52, 53] as:

- Shower particle: It is due to tracks having $g \leq 1.4g_p$, where g is the measured grain density and g_p corresponds to the grain density of the minimum ionizing track. The shower particles are mainly pions (more than 90%) [10, 52–54] having kinetic energy (K.E) > 70 MeV. They have relative velocity $\beta \geq 0.7$. Adamovich et al reported that pions are regarded as the major fraction part of produced particles [54]. They consider the shower particles as pions [54]. At most, the contaminations are not more than 10% (p, baryons, and K–mesons). However, we do not say that the shower particles give rigorous estimation of pions, but they can equilibrate the dominance of the pion production mechanism. Their multiplicity is denoted by n_s . The forward and backward emitted shower particles multiplicities are denoted by n_s^f and n_s^b , respectively.
- Grey particle: It is due to tracks with range > 3 mm and $1.4g_p < g < 4.5g_p$. The grey particles consist mainly of protons knocked–out from the target nucleus. Their energy spectrum is ranged as $26 < \text{K.E} \leq 400$ MeV. Their multiplicity is denoted by N_g .
- Black particle: It is due to tracks having short range ≤ 3 mm and $g > 4.5g_p$. These particles are mainly evaporated target protons with $\text{K.E} \leq 26$ MeV. Their multiplicity is denoted by N_b .
- The grey and black particles together amount the group of heavily ionizing target fragments denoted by $N_h = N_g + N_b$.
- Projectile fragments are those isotopes fragmented from projectile and emitted in the narrow forward cone with θ_{lab} given by the Fermi momentum. Their rapidity is above half of the incident beam rapidity. They are identified as singly, doubly and multiply charged nuclear isotopes.

The nuclear emulsion is a homogeneous mixture of different nuclei. According to the target size, the statistical events are classified into groups correspond to the interactions with H, CNO (the light target),

Em (the emulsion mixture as a whole), and AgBr (the heavy target). The effective mass numbers of these target groups are 1, 14, 70, and 94, respectively. The discrimination of the effective target in a certain interaction can not be directly. Depending on the heavily ionizing target fragment multiplicity, Florian's method [55] is applied in target separation. A detailed example of the target separation is explained widely in Ref. [51].

3.2. Statistical Details

In this experiment the interaction probability with each group is simulated theoretically on the basis of the Glauber's approach [46]. The simulated probabilities are listed in Table (2). Multiplying each probability by the total no of events (Em category), the statistical fraction corresponding to each target is obtained. The measured statistics are listed in Table (3) within round brackets. The MFM simulation of each interaction is run for 10000 events. Some of the obtained simulated events are mixed by those due to elastic scattering, electromagnetic dissociation, and with zero multiplicities. They are excluded from the total 10000 simulated events per interaction to obtain the statistical numbers listed in Table (3) within squared brackets.

Table (2): Interaction probabilities with emulsion nuclei simulated from Glauber's approach.

Projectile	^4He	^{16}O	^{32}S
H	5.24%	8.35%	9.99%
CNO	29.87%	31.66%	35.12%
AgBr	64.89%	59.99%	54.89%

Table (3): Statistical events of the present interactions.

Projectile	^4He	^{16}O	^{32}S
H	(57) [3571]	(47) [2816]	(69) [2321]
CNO	(325) [9860]	(493) [8077]	(228) [7851]
Em	(1092) [10000]	(1473) [9999]	(649) [9991]
AgBr	(710) [10000]	(933) [9999]	(352) [9983]

4. Results and Discussion

4.1. Nuclear Interactions Characteristics

The total scanned lengths (L) of the beams, the number of inelastic interaction events (N), and the measured mean free paths (λ) are listed in Table (4). The simulated mean free paths according to Glauber's approach [46] are placed in round brackets. The total NN inelastic interaction cross section at Dubna energies is taken 44.7 mb [56] for the code input parameters. B is the slope of the differential NN elastic scattering cross section at zero momentum transfer (GeV/c)⁻². Using B iteration in the code, the best λ values can be obtained. To examine the accuracy of the present measurements, the experimental results are compared with those of other labs [57, 58]. For more confirmation, different types of emulsion also are used in comparison, as NIKFI-BR2, FUJI, and ILFORD G5. To confirm the independence of the mean free path on the energy, different values of E_{lab} are introduced. From Table (4) the mean free path decreases against the projectile size. Within statistical errors, the present experimental data agree with the corresponding simulated ones with uncertainty of 0.03, 0.85, and 0.06 standard deviation (SD) for ^4He , ^{16}O , and ^{32}S , respectively. Depending on the energy within statistical errors, the difference between the

two values of λ for ${}^4\text{He}$ is 0.3 SD. For ${}^{16}\text{O}$ the maximum difference between the 5 values of λ is 2.1 SD. For ${}^{32}\text{S}$ the difference between the two values of λ is 1.3 SD. Hence, one can say that the mean free path is insensitive to the energy.

Table (4): Data of ${}^4\text{He}$, ${}^{16}\text{O}$, and ${}^{32}\text{S}$ beams interacting in nuclear emulsions.

Projectile	$E_{\text{lab}}A$ GeV	L m	N events	λ cm	B	Emulsion Type	Ref.
${}^4\text{He}$	2.1	416.5	2006	20.16 ± 0.44	–	NIKFI-BR2	[19]
	3.7	217.6	1092	19.93 ± 0.60 (19.95)	5.2	NIKFI-BR2	Present Work
${}^{16}\text{O}$	3.7	187	1473	12.70 ± 0.33 (12.42)	3.9	NIKFI-BR2	Present Work
		357.689	2960	12.08 ± 0.22	–	NIKFI-BR2	[57]
	60	119.21	910	13.10 ± 0.43	–	FUJI	[51]
	200	103.5	802	12.90 ± 0.50	–	ILFORD G5	[51]
		–	–	–	12.30 ± 0.30	–	BR-2
${}^{32}\text{S}$	3.7	61.98	649	9.55 ± 0.34 (9.57)	3.8	NIKFI-BR2	Present Work
	200	125.47	1391	9.02 ± 0.20	–	FUJI	[18]

The total cross section of the inelastic interactions of 3.7A GeV ${}^4\text{He}$, ${}^{16}\text{O}$, and ${}^{32}\text{S}$ with different emulsion nuclei is correlated with the total system size in Fig. (1).

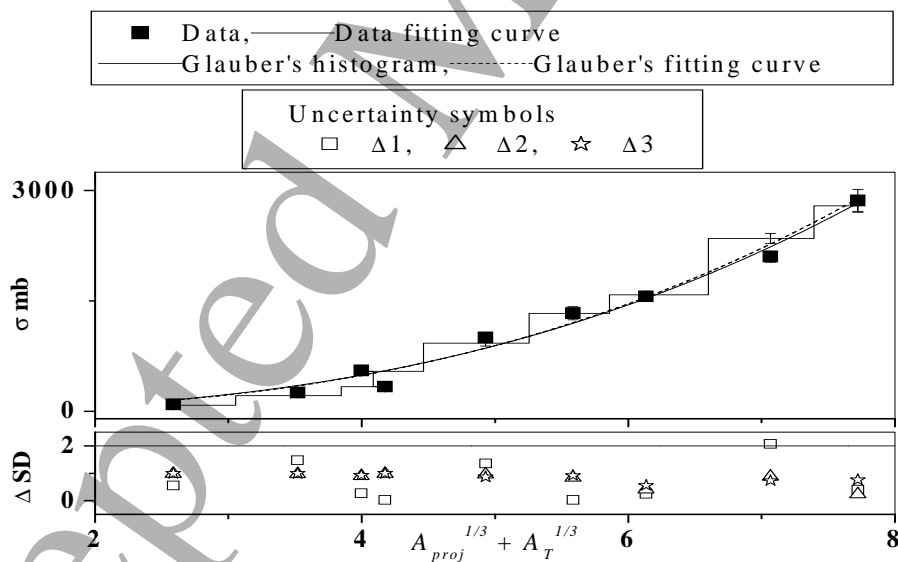


Fig. (1): Inelastic interaction cross section of 3.7A GeV ${}^4\text{He}$, ${}^{16}\text{O}$, and ${}^{32}\text{S}$ in nuclear emulsion.

From the figure, both the experimental data and Glauber's approach are approximated by the power law relation Eq. (8). In the figure $\Delta 1$, $\Delta 2$, and $\Delta 3$ are the differences between the (data and Glauber's approach), (data and its fitting), and (Glauber's approach and its fitting), in units of SD respectively. All the differences often are less than 2 SD. This reflects the goodness of approximation in Eq. (8).

$$\sigma = 11.9(A_{proj}^{\frac{1}{3}} + A_T^{\frac{1}{3}})^{2.7} \text{ mb} \quad (8)$$

4.2. Backward Emitted Shower Particle

The multiplicity distributions of the backward emitted shower particle in 3.7A GeV ${}^4\text{He}$, ${}^{16}\text{O}$, and ${}^{32}\text{S}$ interactions with emulsion nuclei are presented in Fig. (2a). From the figure, the decay shape is a characteristic for all system sizes. This implies that a single source is responsible for the backward production.

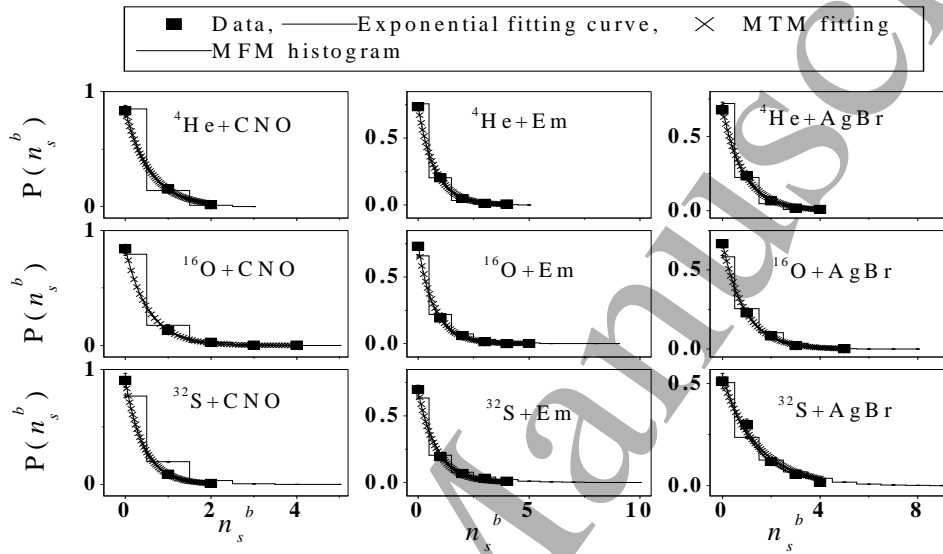


Fig. (2a): Multiplicity distributions of the backward emitted shower particle in 3.7A GeV ${}^4\text{He}$, ${}^{16}\text{O}$, and ${}^{32}\text{S}$ interactions with emulsion nuclei.

4.2.1. Exponential decay fitting

The distributions are approximated by the exponential decay law Eq. (9), where λ_s^b and p_s^b are fitting parameters. They are listed in Table (6). The goodness of this fitting is confirmed in Fig. (2b) by $\Delta 1$, which is the difference between the fitted distributions and the data.

$$P(n_s^b) = p_s^b e^{-\lambda_s^b n_s^b} \quad (9)$$

Table (6): Fitting parameters of Eq. (9).

Projectile		${}^4\text{He}$	${}^{16}\text{O}$	${}^{32}\text{S}$
Parameter	Target			
p_s^b	CNO	0.84 ± 0.05	0.84 ± 0.04	0.90 ± 0.06
	Em	0.74 ± 0.03	0.74 ± 0.02	0.68 ± 0.03
	AgBr	0.69 ± 0.03	0.67 ± 0.03	0.54 ± 0.04
λ_s^b	CNO	1.83 ± 0.12	1.84 ± 0.05	2.32 ± 0.20
	Em	1.35 ± 0.05	1.39 ± 0.04	1.15 ± 0.05
	AgBr	1.16 ± 0.05	1.10 ± 0.04	0.77 ± 0.05
χ^2/dof	CNO	0	0.25	0
	Em	0.43	1.48	0.67
	AgBr	0.49	0.25	0.62

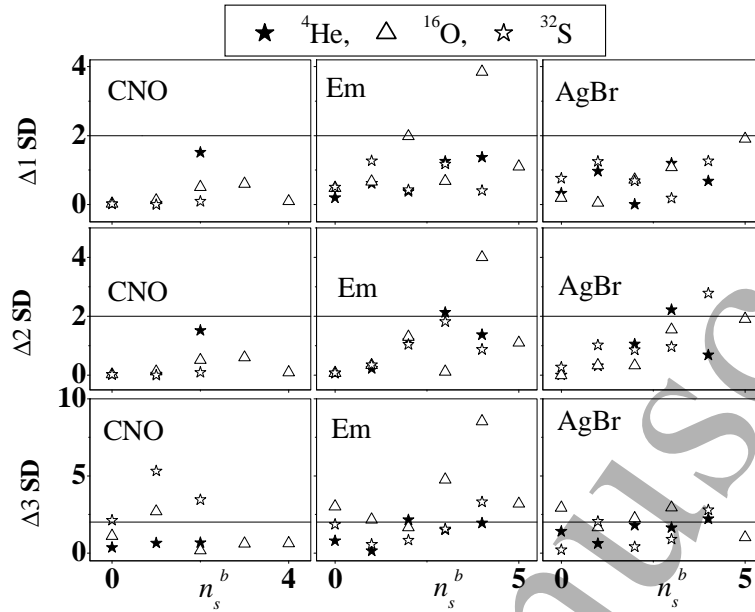


Fig. (2b): Systematic uncertainty of the fitting and models applied on the distributions of Fig. (2a).

4.2.2. MTM fitting for backward shower particle multiplicity distributions

Eq. (6) reproduces the data in the framework of MTM with $j = 1$ and $m_j = 1$, as shown in Fig. (2a). The fitting parameters k_1 and $\langle n_{i1} \rangle$ are listed in Table (7) where k_1 is a normalization factor. The goodness of this fitting is confirmed in Fig. (2b) by $\Delta 2$ values, which is the difference between the fitted distributions and the data. It often is not more than 2 SD. One subgroup including single source ($m_j = 1$) is adequate to predict the backward pion production, irrespective of the system size. Therefore, Eq. (6) is reduced to Eq. (1), which is characterized by a single source. From the table, both k_1 and $\langle n_{i1} \rangle$ increase with the target size. Apart from the observed remarkable deviations for ^{32}S interactions with CNO and AgBr nuclei, which can be attributed to statistical reasons, the parameters nearly are insensitive to the projectile size. Comparing Eq. (1) with Eq. (9), they seem equivalent. Finally, one concludes that both MTM fitting and the exponential decay one can be applied well to reproduce the backward emitted shower particle multiplicity distribution. This production system is characterized by single source associated with target fragmentation.

Table (7): Parameters of MTM fitting run in Fig. (2a).

Projectile		^4He	^{16}O	^{32}S
Parameter	Target			
k_1	CNO	0.48 ± 0.02	0.45 ± 0.01	0.39
	Em	0.56 ± 0.01	0.56 ± 0.01	0.57 ± 0.02
	AgBr	0.61 ± 0.02	0.62 ± 0.01	0.76 ± 0.06
$\langle n_{i1} \rangle$	CNO	0.58 ± 0.03	0.54 ± 0.01	0.43
	Em	0.76 ± 0.01	0.76 ± 0.01	0.81 ± 0.03
	AgBr	0.91 ± 0.03	0.94 ± 0.01	1.46 ± 0.13
χ^2/dof	CNO	0	5×10^{-6}	0
	Em	10^{-5}	6.7×10^{-6}	6×10^{-5}
	AgBr	4×10^{-5}	10^{-5}	3×10^{-4}

4.2.3. MFM simulations of the backward shower particle multiplicity distributions

The MFM simulations of the backward emitted shower particle distributions are presented in Fig. (2a) by histograms. The simulations often have longer tails than the data. The goodness of simulations is examined in Fig. (2b) by the difference $\Delta 3$. Apart from the longer simulated tails, $\Delta 3$ nearly does not exceed 2 SD for ${}^4\text{He}$ interactions. For ${}^{16}\text{O}$ interactions $\Delta 3$ often exceeds 2 SD. For ${}^{32}\text{S}$ interactions with Em and AgBr, $\Delta 3$ often is not more than 2 SD. Thus, the MFM predicts the backward emitted shower particle multiplicity distributions qualitatively.

4.3. Forward Emitted Shower Particle

The forward emitted shower particle multiplicity distributions of 3.7A GeV ${}^4\text{He}$, ${}^{16}\text{O}$, ${}^{32}\text{S}$ interactions with emulsion nuclei are presented in Fig. (3a).

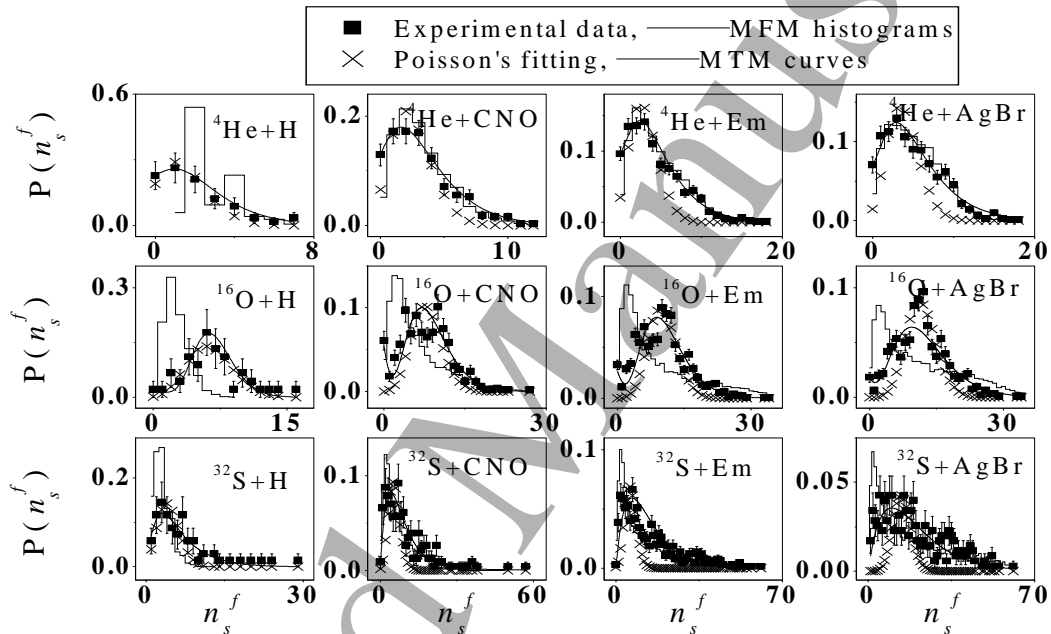


Fig. (3a): Multiplicity distributions of the forward emitted shower particle in 3.7A GeV ${}^4\text{He}$, ${}^{16}\text{O}$, and ${}^{32}\text{S}$ interactions with emulsion nuclei.

Unlike the characteristic decay shapes observed in the backward emitted shower particle multiplicity distributions, the distributions are characterized by peaking shapes herein. This characteristic shape is due to multisource superposition, where different sets of impact parameters are enclosed in the system. The multiplicity range increases with the system size. The increase is more valuable w. r. t. the projectile size than the target size. In ${}^4\text{He}$ -nucleus collisions, the distributions transform gradually with the target size from hill to mountain shape. They can not have the bell shapes similar to Gaussian distributions. Hence, the isotropy of multisource contributions does not exist. In ${}^{16}\text{O}$ -nucleus collisions, the distributions nearly are symmetric about the peaks, apart from qualitative tails at higher multiplicities for heavier targets. This indicates the isotropy of the multisource contributions. In ${}^{32}\text{S}$ -nucleus collisions, the behavior is nearly similar to that in ${}^4\text{He}$ -nucleus collisions. In Fig. (3b) the goodness of the fitting is examined by the differences between the (data and the Poisson's fitting) and (data and MTM fitting). These differences are denoted $\Delta 1$ and $\Delta 2$, respectively. The difference between the data and MFM simulations is $\Delta 3$.

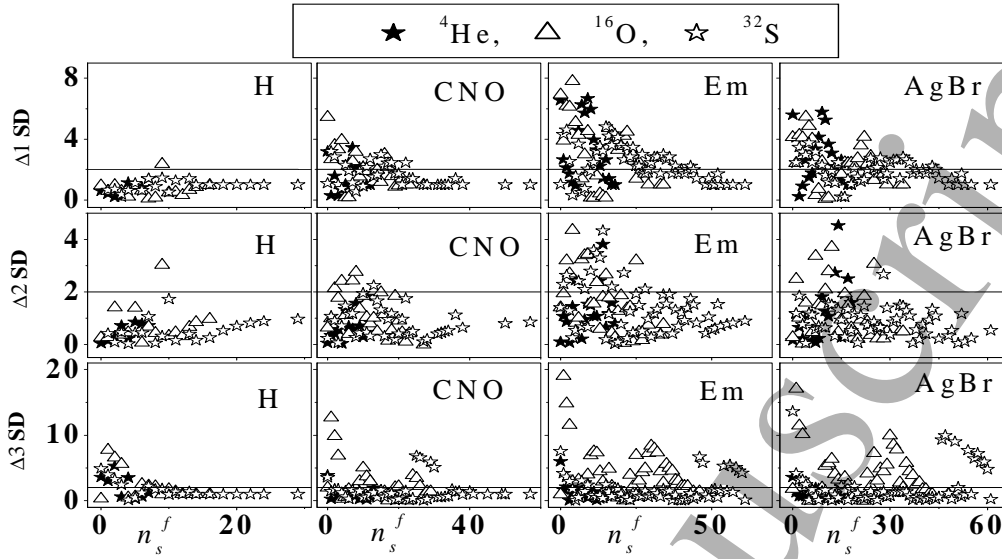


Fig. (3b): Systematic uncertainty of the fitting and models applied on the distributions of Fig. (3a).

4.3.1. Poisson's fitting

The Poisson's law Eq. (10) fits the distributions. The values of the normalization factor (p_s^f) are listed in Table (8). The fitted average multiplicity ($\langle n_s^f \rangle_{\text{Poisson}}$) will be presented diagrammatically in other section to compare with the measured one. From Fig. (3a) and Fig. (3b), one can notice that the Poisson's law has a better fitting for the data at smaller system sizes than larger ones. For larger system sizes $\Delta 1$ often exceeds 2 SD at the intermediate multiplicity region. The deviation may be due to the contribution of some nonthermal processes responsible for pion production in most central collisions [59], which are enclosed through averaging over different impact parameters. It may be also due to statistical reasons. We expect that the pion produced in nonthermal processes at the present energy is associated with the target source pions, which are possible to be emitted in the 4π space. Their contribution to the FHS may enhance the observed deviation. On the other hand, the contribution of different hadrons, other than pions (less than 10%), to the shower particle multiplicity can also share in the observed deviation. Hence, the Poisson's fitting can be more successful for small collision systems.

$$P(n_s^f) = p_s^f \frac{\langle n_s^f \rangle_{\text{Poisson}}^{n_s^f}}{n_s^f!} e^{-\langle n_s^f \rangle_{\text{Poisson}}} \quad (10)$$

Table (8): Fitting parameters of Eq. (10).

Projectile		${}^4\text{He}$	${}^{16}\text{O}$	${}^{32}\text{S}$
Parameter	Target			
p_s^f	H	0.88 ± 0.10	0.89 ± 0.08	0.74 ± 0.08
	CNO	0.82 ± 0.07	0.72 ± 0.08	0.55 ± 0.07
	Em	0.72 ± 0.07	0.70 ± 0.06	0.43 ± 0.05
	AgBr	0.71 ± 0.08	0.74 ± 0.06	0.40 ± 0.06
χ^2/dof	H	2×10^{-4}	5.5×10^{-5}	5×10^{-5}
	CNO	9×10^{-5}	3×10^{-5}	2×10^{-5}
	Em	5×10^{-5}	1.2×10^{-5}	5×10^{-6}
	AgBr	6×10^{-5}	8.6×10^{-6}	5.9×10^{-6}

4.3.2. MTM fitting for forward shower particle multiplicity distributions

The distributions are fitted by MTM. The fitting parameters are listed in Table (9). From Fig. (3b), Δ^2 often does not exceed 2 SD over the major multiplicity range.

Table (9): Parameters of MTM fitting run in Fig. (3a)

Projectile		${}^4\text{He}$	${}^{16}\text{O}$	${}^{32}\text{S}$	
Target	Parameter				
H	j = 1	k_1	0.88	0.95	0.805
		m_1	2	10	2
		$\langle n_{i1} \rangle$	1.31 ± 0.08	0.69 ± 0.03	3.477 ± 0.363
	j = 2	k_2	0.12	0.05	0.195
		m_2	1	1	3
		$\langle n_{i2} \rangle$	0.52 ± 0.05	1.77 ± 1.99	1.308 ± 0.312
	χ^2/dof		9×10^{-5}	8×10^{-5}	2×10^{-5}
CNO	j = 1	k_1	0.90	0.90	0.83
		m_1	2	5	2
		$\langle n_{i1} \rangle$	1.92 ± 0.06	1.75 ± 0.07	3.99 ± 0.26
	j = 2	k_2	0.10	0.04	0.17
		m_2	1	2	1
		$\langle n_{i2} \rangle$	0.77 ± 0.06	0.01	23.32 ± 18.37
	j = 3	k_3	–	0.06	–
		m_3	–	1	–
		$\langle n_{i3} \rangle$	–	1.11 ± 0.33	–
	χ^2/dof		10^{-5}	10^{-5}	4×10^{-6}
Em	j = 1	k_1	0.95	0.90	1.08
		m_1	2	5	2
		$\langle n_{i1} \rangle$	2.40 ± 0.07	2.21 ± 0.07	6.68 ± 0.32
	j = 2	k_2	0.05	0.05	–
		m_2	1	3	–
		$\langle n_{i2} \rangle$	0.52 ± 0.05	0.01	–
	j = 3	k_3	–	0.05	–
		m_3	–	1	–
		$\langle n_{i3} \rangle$	–	1.89 ± 0.79	–
	χ^2/dof		4×10^{-6}	4.5×10^{-6}	1.9×10^{-6}
AgBr	j = 1	k_1	0.97	0.90	0.965
		m_1	2	4	2
		$\langle n_{i1} \rangle$	2.81 ± 0.09	3.17 ± 0.14	9.981 ± 0.495
	j = 2	k_2	0.03	0.05	–
		m_2	1	2	–
		$\langle n_{i2} \rangle$	0.44 ± 0.05	0.01	–
	j = 3	k_3	–	0.05	–
		m_3	–	1	–
		$\langle n_{i3} \rangle$	–	2.89 ± 1.76	–
	χ^2/dof		5×10^{-6}	4.8×10^{-6}	10^{-6}

From Table (9), in all collisions induced by ${}^4\text{He}$ nucleus, and in the collisions of ${}^{32}\text{S}$ with the light groups of nuclei (H and CNO), two subgroups of sources are contributed. One of both is dominant, where its weight factor is more than 0.8. It always consists of 2 sources. In ${}^{32}\text{S}$ collisions with the heavy groups of

nuclei (Em and AgBr), one subgroup having two sources is contributed. In ^{16}O -nucleus collisions the production system often is sourced by 3 subgroups. One of them is dominant, where its weight factor is not less than 0.9. The main subgroups are expected to be due to different pionization sources (Δ , ρ , ω , η , η' , and direct reactions). The minor subgroups may be due to the contribution of less than 10% hadrons other than pions to the forward emitted shower particle multiplicity. The fraction of the target source pions emitted in the FHS may be enclosed in the minor subgroups or in the main ones. Hence in this production system, while the number of sources and subgroups depend on the system size, the projectile size is more effective.

4.3.3. MFM Simulations of forward shower particle multiplicity distributions

From Fig. (3b), $\Delta 3$ often is greater than 2 SD for the interactions of ^4He and ^{16}O with H. For the interactions of ^4He and ^{32}S with heavier target nuclei, $\Delta 3$ often does not exceed 2 SD over the major multiplicity range. Hence, the MFM simulations can predict the forward emitted shower particle multiplicity distributions in ^4He and ^{32}S interactions with nuclei other than H. It does not succeed in ^{16}O -Nucleus interactions.

4.4. Systematic Parameterization

4.4.1. Dependence of $\langle n_s^f \rangle$ on $\langle n_s^b \rangle$

The two components of shower particle multiplicity $\langle n_s^f \rangle$ and $\langle n_s^b \rangle$ are correlated together in Fig. (4) for 3.7A GeV ^4He , ^{16}O , and ^{32}S interactions with emulsion nuclei.

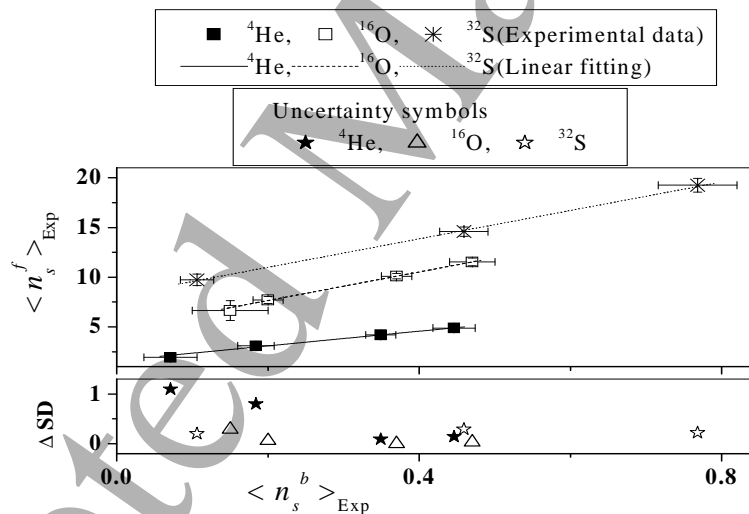


Fig. (4): Correlation between the forward and backward emitted shower particle multiplicities in 3.7A GeV ^4He , ^{16}O , and ^{32}S interactions with emulsion nuclei.

The data are fitted by linear relation law. The linear fitting has correlation coefficient ($r \sim 0.996, 0.999$, and 0.999 for ^4He , ^{16}O , and ^{32}S data, respectively). In the same respect, the intercept parameter of the line segments is 1.62 ± 0.16 , 4.78 ± 0.14 , and 8.15 ± 0.22 . The fact that the line does not pass through the origin, reflects the projectile size dependence of the multiplicity. In the same respect, the slope is 7.37 ± 0.48 , 14.38 ± 0.40 , and 14.29 ± 0.46 . The larger slope reflects the increased amount of nuclear matter involved in the interaction. The lines corresponding to ^{16}O and ^{32}S nearly have the same slopes within experimental errors with difference of 0.1 SD. This constancy may imply a limitation of the involved nuclear matter

size for the dependence on the backward emitted shower particle multiplicity for $A_{proj} \geq 16$. On average the slope is ~ 14.34 for ^{16}O and ^{32}S data. This value is bigger about 1.95 orders of magnitude than that of ^4He value. The goodness of the fitting is presented in the figure by the difference between the data and the fitting within errors (Δ). Δ always is < 2 SD.

The intercept is approximated as a linear function of the projectile size in Fig. (5) with $r \sim 0.997$. The linear fitting of Fig. (5) has intercept parameter $\sim 0.82 \pm 0.32$ and slope $\sim 0.24 \pm 0.01$. The goodness of the fitting is presented in the figure by the difference between the intercepts and the fitting within errors (Δ). Δ always is < 2 SD. Hence, we can write the correlation in the form of the linear law Eq. (11). We can not confirm the universality of Eq. (11), where the onset of the slope limitation before $A_{proj} = 16$ is not checked up in this experiment.

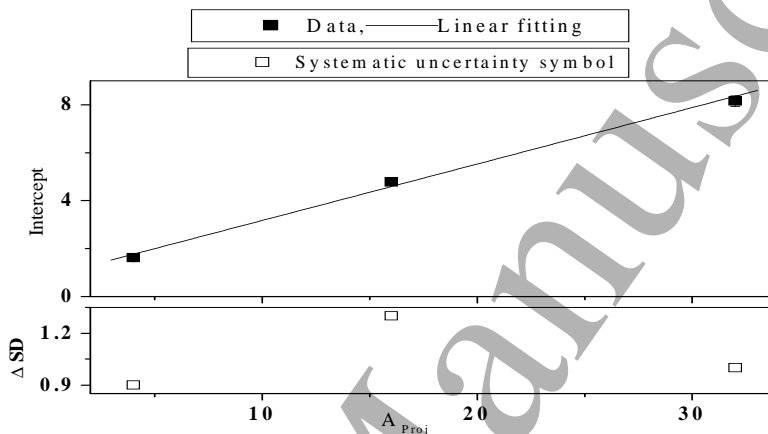


Fig. (5): Intercepts of the line segments presented in Fig. (4) as a function of the projectile size.

$$\begin{cases} \langle n_s^f \rangle_{Exp} = 0.82 + 0.24A_{proj} + 7.37 \langle n_s^b \rangle_{Exp} \text{ for } ^4\text{He} \\ \langle n_s^f \rangle_{Exp} = 0.82 + 0.24A_{proj} + 14.34 \langle n_s^b \rangle_{Exp} \text{ for } ^{16}\text{O} \text{ and } ^{32}\text{S} \end{cases} \quad (11)$$

4.4.2. Dependence of the average multiplicities on the system size

The measured average shower particle multiplicity ($\langle n_s^f \rangle_{Exp}$ and $\langle n_s^b \rangle_{Exp}$) in 3.7A GeV ^4He , ^{16}O , and ^{32}S interactions with emulsion nuclei is parameterized as a function of the target mass number in Fig. (6). From the figure, $\langle n_s^f \rangle_{Exp}$ and $\langle n_s^b \rangle_{Exp}$ increase linearly with A_T . The goodness of the linear fitting is examined by the difference between the measured values and the fitted ones, $\Delta 1$ SD. It always does not exceed 2 SD. The measured values are compared with the simulated ones of MFM, Poisson's fitting, and MTM fitting. $\Delta 2$, $\Delta 3$, and $\Delta 4$ are the differences of Poisson's fitted, MTM fitted, and MFM values w. r. t. the measured ones in units of SD, respectively. The Poisson's fitted values may agree with measurements for ^4He and ^{16}O data, where $\Delta 2$ for them is not more than 2 SD. The MTM fitted values have a good agreement with measurements, where $\Delta 3$ often is not more than 2 SD. The MFM simulation agrees with ^4He data only, where $\Delta 4$ nearly is more than 2 SD for other projectiles data. The linear relation has fitting parameters listed in Table (10). From the table, the slopes in the FHS are greater than those in BHS 8 times at least. The intercepts in the FHS are greater than those in BHS 23 times at least. This reflects that the production in the BHS is very low w. r. t. the FHS. In FHS, the intercept parameters for ^{16}O and ^{32}S interactions are nearly the same, where they differ with 0.3 SD within statistical errors. On average the intercept is ~ 7.1 . This intercept value nearly is 3 times higher than that of ^4He interaction. The slope increases with the projectile size. Hence, we can suggest that the nuclear matter size is nearly

the same in ^{16}O and ^{32}S collisions with the light target nuclei. In BHS the behavior is different, where the intercept nearly is the same for ^4He and ^{16}O . It differs with 0.4 SD within statistical errors. The slope parameters also are the same. A slight deviation is observed for ^{32}S data due to statistical reasons. Anyhow, the behavior in the BHS changes insignificantly with the projectile size.

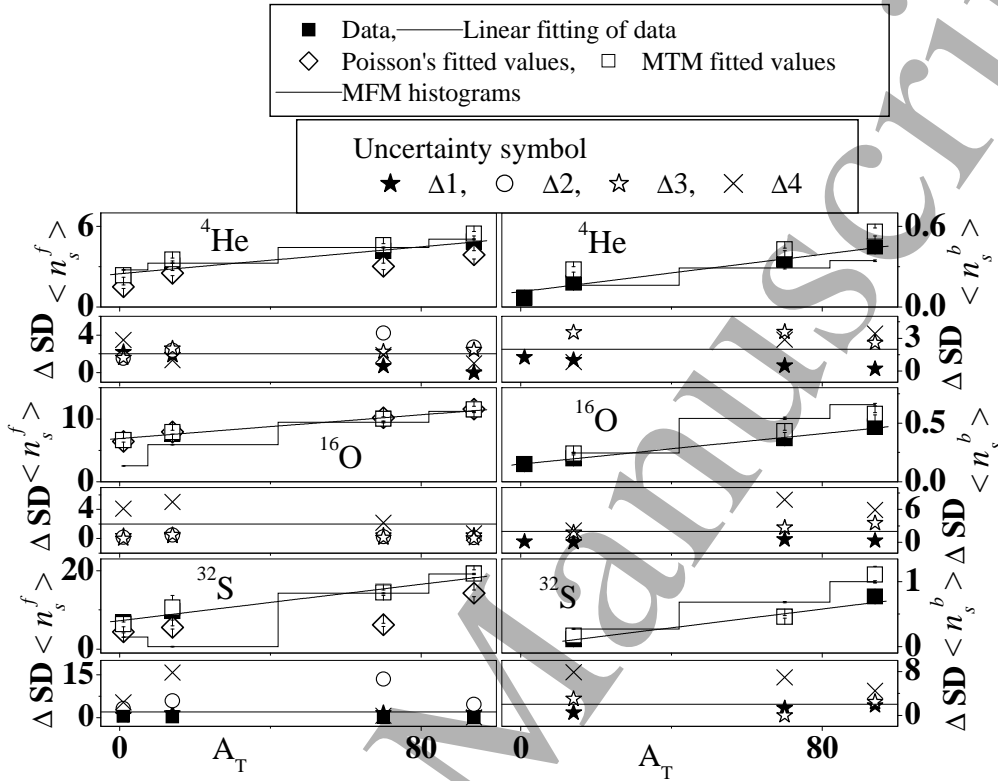


Fig. (6): Average shower particle multiplicity in 3.7A GeV ^4He , ^{16}O , and ^{32}S interactions with emulsion nuclei as function of the target mass number.

Table (10): Fitting parameters of line segments shown in Fig. (6).

Projectiles	Intercept			Slope		
	FHS	BHS	r	FHS	BHS	r
^4He	2.48 ± 0.29	0.11 ± 0.02	0.964	0.025 ± 0.005	0.003	0.988
^{16}O	6.93 ± 0.22	0.15 ± 0.01	0.995	0.047 ± 0.003	0.003	0.997
^{32}S	7.27 ± 0.98	0.003 ± 0.060	0.980	0.116 ± 0.017	0.007 ± 0.001	0.986

The slope is approximated as a linear function of the projectile size in Fig. (7) with $r \sim 0.93594$. The linear fitting of Fig. (7) has intercept = 0.01233 ± 0.01259 and slope = $0.0023 \pm 8.7 \times 10^{-4}$. The goodness of this fitting is presented in the figure by the difference between the slopes and the fitting within errors (Δ). Δ always is < 2 SD. Hence, we can write the correlation in the form of the linear law Eq. (12). We can not confirm the universality of Eq. (12), where the onset of the intercept limitation before $A_{\text{proj}} = 16$ is not checked up in this experiment.

$$\begin{cases} \langle n_s^f \rangle_{\text{Exp}} = 2.48 + 0.01233A_T + 0.0023A_{\text{proj}}A_T & \text{for } ^4\text{He} \\ \langle n_s^f \rangle_{\text{Exp}} = 7.1 + 0.01233A_T + 0.0023A_{\text{proj}}A_T & \text{for } ^{16}\text{O} \text{ and } ^{32}\text{S} \end{cases} \quad (12)$$

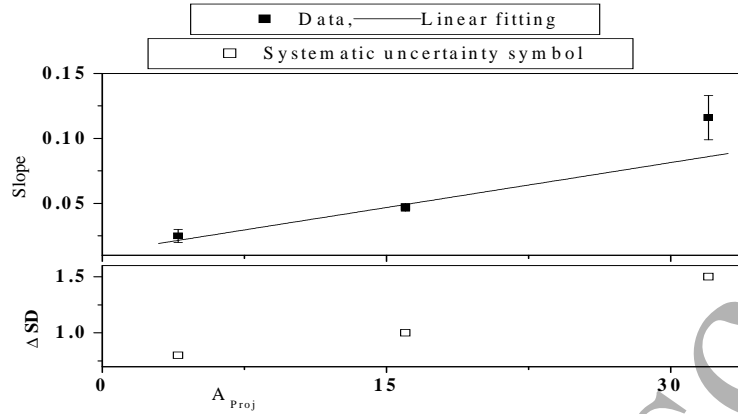


Fig. (7): Slopes of the line segments presented in Fig. (6) associated with the FHS as a function of the projectile size.

4.4.3. Dependence of the production probabilities on the system size

The production probability of the forward or backward emitted shower particle is defined as the number of events having $n_s^f > 0$ or $n_s^b > 0$, respectively normalized to the total number of events in percent. In the same respect, they are denoted as $P(n_s^f > 0)\%$ and $P(n_s^b > 0)\%$. This probability is parameterized as a function of the target size for 3.7A GeV ^4He , ^{16}O , and ^{32}S interactions with emulsion nuclei in Fig. (8). From the figure, the probability increases linearly with the target size. In the FHS the linear fitting has intercept parameter = 83.95 ± 2.51 , 93.46 ± 0.86 , and 98.09 ± 1.99 according to ^4He , ^{16}O , and ^{32}S , respectively. This increase indicates a dependence on the projectile size. In the same respect, the slope parameter is 0.09 ± 0.03 , 0.05 ± 0.01 , and, 0.01 ± 0.03 .

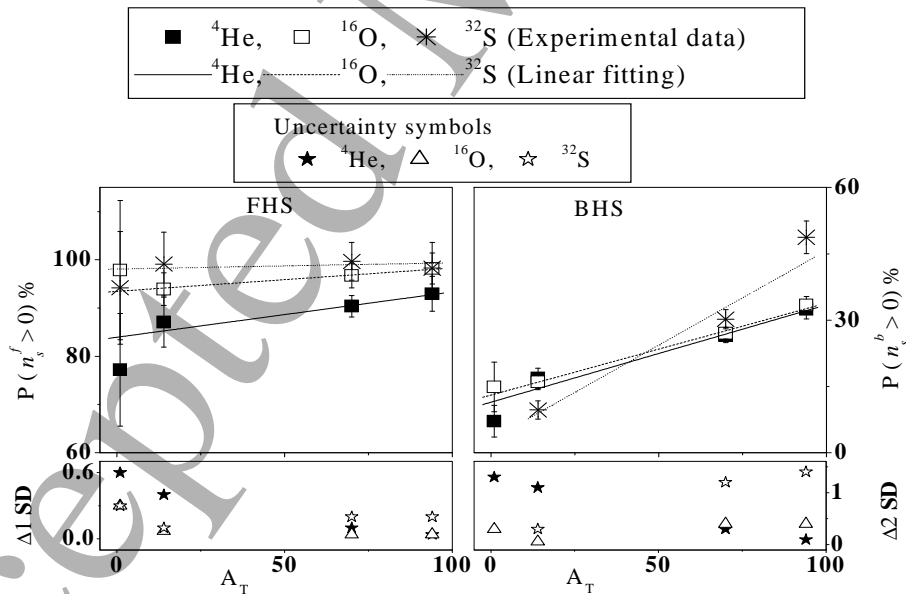


Fig. (8): Dependence of the shower particle production probability in 3.7A GeV ^4He , ^{16}O , and ^{32}S interactions with emulsion nuclei on the target size.

The slope nearly is constant within experimental errors, where the maximum difference is 1.9 SD. This constancy indicates that though there is a considerable dependence on the target size, its role is respected in determination of the nuclear matter size only not in particle sourcing. The slope, on average, is ~ 0.05 . In the same respect, r is ~ 0.89 , 0.94 , and 0.31 . The goodness of the fitting is examined by $\Delta 1$. $\Delta 1$ is the difference between the data and the corresponding fitted values in units of SD within errors. From the figure, $\Delta 1$ always is < 2 SD. The intercept values are parameterized as a function of the projectile mass number in Fig. (9). The allometric fitting in Fig. (9) is presented by the power law Eq. (13). It has $\chi^2/\text{dof} = 0$. The fitting parameters c and d are $\sim 75.72 \pm 0.42$ and 0.075 ± 0.002 , respectively. The difference (Δ) between the intercept and the corresponding fitted values always is < 2 SD. Thus, the final relation can be written as Eq. (14). Eq. (14) can be considered a universal law for nuclear collisions at 3.7A GeV.

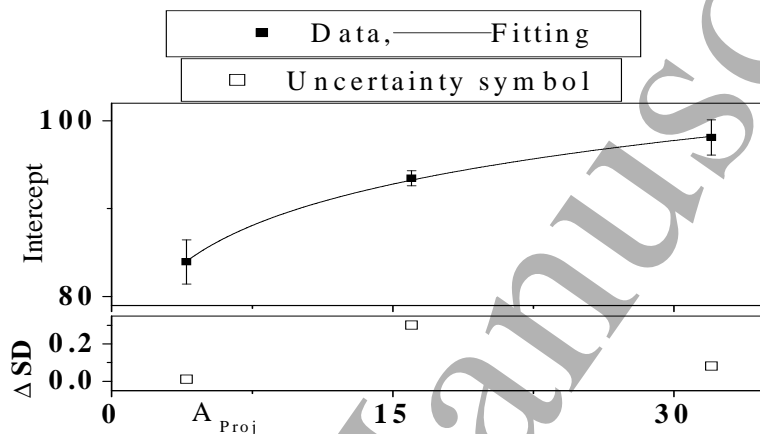


Fig. (9): Parameterization of the intercept values of the lines presented in FHS inset of Fig. (8) as a function of projectile mass number.

$$\text{Intercept} = cA_{proj}^d \quad (13)$$

$$P(n_s^f > 0)\% = 75.72A_{proj}^{0.075} + 0.05A_T \quad (14)$$

In the BHS the linear fitting has intercept parameter $\sim 11.42 \pm 2.50$, 13.03 ± 0.95 , and 2.96 ± 5.01 according to ${}^4\text{He}$, ${}^{16}\text{O}$, and ${}^{32}\text{S}$, respectively. The maximum difference in these values is ~ 2 SD within experimental errors. On average, the intercept is ~ 9.14 , irrespective of the projectile size. In the same respect, the slope parameter is 0.22 ± 0.04 , 0.21 ± 0.01 , and, 0.43 ± 0.09 . The maximum difference in the slopes is 2.4 SD within experimental errors. Anyhow, this highness is not valuable. It may be due to statistical reasons. This can be confirmed from the values of $\Delta 2$ which is the difference between the data and the corresponding fitting values within errors in units of SD. $\Delta 2$ always is < 2 SD. The average slope is ~ 0.29 . The dependence on the target size is clear while on the projectile size is insignificant. Hence, one can write a universal law for this production in Eq. (15).

$$P(n_s^b > 0)\% = 9.14 + 0.29A_T \quad (15)$$

5. Summary and Conclusion

- In summary the shower particle multiplicity characteristics in 3.7A GeV ${}^4\text{He}$, ${}^{16}\text{O}$, and ${}^{32}\text{S}$ interactions with emulsion nuclei provide insight into the final state hadron production at few GeV region. Minimum bias data sample are selected randomly at average impact parameter.
- The applied Glauber's approach simulation code predicts the mean free path (λ) successfully. λ is independent on the energy. The total inelastic interaction cross section is approximated in units of mb by the universal law, $\sigma = 11.9(A_{proj}^{\frac{1}{3}} + A_T^{\frac{1}{3}})^{2.7}$, which depends only on the system size.

- 1
2
3
4
5
6 - The backward emitted shower particle multiplicity distributions always are characterized by
7 decay shape, irrespective of the system size. The nuclear limiting fragmentation hypothesis is
8 regarded in this production system. The distributions are approximated by exponential law having
9 decay constant, which is dependent on the target nucleus. The MTM indicates that a single source
10 is responsible for this production system. The exponential decay and MTM fittings nearly have
11 equivalent goodness to reproduce the distributions. The MFM simulation qualitatively reproduces
12 the distributions. The observed deviations of the simulation from the data may be attributed to
13 statistical reasons, whereas the model modification for nuclear destruction seems adequately
14 reasonable to predict this production system.
- 15 - The forward emitted shower particle multiplicity distributions are characterized by peaking
16 shaped curves. The broadening and symmetry of the curves about peak position depend on the
17 system size. The distributions are fitted by Poisson's law where the average multiplicities are
18 obtained as fitting parameters. The Poisson's shapes deviate from the data at higher multiplicities
19 due to statistical reasons. At the intermediate multiplicities the deviations may be due to statistical
20 reasons and/or averaging over all impact parameters. The contributions of nonthermal process to
21 pion production in extreme central collisions also are suggested to be responsible for the
22 deviation. Anyhow, the Poisson's fitting may be sustainable for small collision systems. The
23 MTM confirms that this production system is multisource superposition. Its fitting gives more
24 successful predictions than Poisson's one, where it can be realized over the sources subgroups
25 enclosed in the system. The predicted number of sources and subgroups depends on the system
26 size. In all system sizes the main subgroup is expected to be mainly due to pionization sources,
27 where its weight factor always exceeds 0.8. The MFM fails to predict the data for collisions with
28 H, in which the intranuclear cascading is improbable. In ^4He collisions with CNO, Em, and AgBr,
29 the MFM succeeds to predict the results. In ^{16}O collisions the MFM fails to predict the data. In ^{32}S
30 collisions the MFM predictions seem better than for ^{16}O ones, especially when the target size
31 increases. The observed deficiencies in the MFM predictions for this hadronization system may
32 be attributed to the model assumption. That is, resonances are the source of the final state hadron
33 in this energy region, while the other sources as the direct reactions are not enclosed. This
34 production is suggested to be hadronization system. It depends on the system size, in which the
35 target nucleus is not a source, but its role does not overstep a participation in the system
36 centrality.
- 37 - The forward emitted shower particle average multiplicity is parameterized empirically as a
38 function of $(A_{\text{Proj}}, \langle n_s^b \rangle)$. It is parameterized also as a function of $(A_{\text{Proj}}, A_{\text{T}})$. The universality of
39 these functions at the present energy may not be confirmed, where the projectile size is not
40 checked up over the range $4 < A_{\text{Proj}} < 16$ in this experiment.
- 41 - The forward emitted shower particle production probability is parameterized empirically as a
42 universal function of $(A_{\text{Proj}}, A_{\text{T}})$ at the present energy. The backward emitted shower particle
43 production probability is parameterized empirically as a universal function of (A_{T}) at the present
44 energy.
45
46

47 6. Acknowledgment

48
49 The authors are grateful to JINR, Dubna, Russia, specially Vekseler and Baldin High Energy
50 Laboratory for supplying us the photographic emulsion plates.
51

52 7. References

- 53
54 [1] R. Stock, Physics Reports 135, 259 (1986).
55 [2] W. Thomé, K. Eggert, K. Giboni, H. Liskén, P. Darriulat, P. Dittmann, M. Holder, K.T. McDonald, H.
56 Albrecht, T. Modis, K. Tittel, H. Preissner, P. Allen, I. Derado, V. Eckardt, H.-J. Gebauer, R. Meinke,
57 P. Seyboth, and S. Uhlig, Nucl. Phys. B129 (1977) 365.
58
59
60

- 1
2
3
4
5
6 [3] C. Y. Wong, Introduction to high-energy heavy ion collisions, 1994, Singapore: World
7 Scientific (1994) 516 p.
8 [4] Ning Yu and Xiaofeng Luo, Eur. Phys. J. A 55, 26 (2019).
9 [5] B. ANDERSSON, G. GUSTAFSON, G. INGELMAN, and T. SJÖSTRAND, Phys. Rep. 97, 31
10 (1983).
11 [6] B. Andersson, G. Gustafson, and B. Nilsson–Almqvist, Nucl. Phys. B 281, 289 (1987).
12 [7] S. Backović, D. Salihagić, Lj. Simić, D. Krpić, S. Drndarević, R. R. Mekhdiyev, A. P. Cheplakov, H.
13 N. Agakishiev, E. N. Kladnitskaya, and S. Yu. Sivoklov, Phys. Rev. C 46, 1501 (1992).
14 [8] G. D. Westfall, J. Gosset, P. J. Johansen, A. M. Poskanzer, W. G. Meyer, H. H. Gutbrod, A. Sandoval,
15 and R. Stock, Phys. Rev. Lett. 37, 1202 (1976).
16 [9] J. Gosset, H. H. Gutbrod, W. G. Meyer, A. M. Poskanzer, A. Sandoval, R. Stock, and G. D. Westfall,
17 Phys. Rev. C 16, 629 (1977).
18 [10] A. Abdelsalam, M. S. El–Nagdy, and B. M. Badawy, Can. J. Phys. 89, 261 (2011).
19 [11] A. M. Baldin, Yad. Fiz. 10, 1201 (1971).
20 [12] A. M. Baldin, N. Giordenescu, V. N. Zubarev, L. K. Ivanova, N. S. Moroz, A. A. Povtoreiko, V. B.
21 Radomanov, and Stavinskiĭ, Sov. J. Nucl. Phys. 20, 629 (1975).
22 [13] Sverker Fredriksson, Phys. Rev. Lett. 45, 1371 (1980).
23 [14] L. S. Schroeder, S. A. Chessin, J. V. Geaga, J. Y. Grossiord, J. W. Harris, D. L. Hendrie, R.
24 Treuhaft, and K. Van Bibber, Phys. Rev. Lett. 43, 1787 (1979).
25 [15] J. V. Geaga, S. A. Chessin, J. Y. Grossiord, J. W. Harris, D. L. Hendrie, L. S. Schroeder, R. N.
26 Treuhaft, and K. Van Bibber, Phys. Rev. Lett. 45, 1993 (1980).
27 [16] M. El–Nadi, A. Abdelsalam, N. Ali–Mossa, Z. Abou–Moussa, Kh. Abdel–Waged, W. Osman, and
28 B. M. Badawy IL Nuovo Cimento A 111, 1243 (1998).
29 [17] A. Abdelsalam, E. A. Shaat, N. Ali–Mossa, Z. Abou–Moussa, O. M. Osman, N. Rashed, W. Osman,
30 B. M. Badawy, and E. El–Falaky, J. Phys. G: Nucl. Part. Phys. 28, 1375 (2002).
31 [18] A. Abdelsalam, B. M. Badawy, and M. Hafiz, J. Phys. G: Nucl. Part. Phys. 39, 105104 (2012).
32 [19] A. Abdelsalam, Z. Abou–Moussa, N. Rashed, B. M. Badawy, H. A. Amer, W. Osman, M. M. El–
33 Ashmawy, and N. Abdallah, Chinese Physics C 39, 094001 (2015).
34 [20] A. Abdelsalam, B. M. Badawy, H. A. Amer, W. Osman, M. M. El–Ashmawy, and N. Abdallah,
35 International Journal of Modern Physics E 27, 1850026 (2018).
36 [21] A. M. Baldin, Part. Nucl. 8, 429 (1977).
37 [22] M. I. Gorenstein and G. M. Zinovjev, Phys. Lett. B 67, 100 (1977).
38 [23] M. I. Gorenstein, V. P. Shelest, and G. M. Zinovjev, Yad. Fiz. 26, 788 (1977) [Sov. J. Nucl. Phys.
39 26, 414, (1977)].
40 [24] I. G. Bogatskaya, C. B. Chiu, M. I. Gorenstein, and G. M. Zinovjev, Phys. Rev. C 22, 209 (1980).
41 [25] H. B. Mathis and Meng Ta–chung, Phys. Rev. C 18, 952 (1978).
42 [26] L. S. Schroeder, S. A. Chessin, J. V. Geaga, J. Y. Grossiord, J. W. Harris, D. L. Hendrie, R.
43 Treuhaft, and K. Van Bibber, Phys. Rev. Lett. 43, 1787 (1979).
44 [27] M. El–Nadi, N. Ali–Mossa, and A. Abdelsalam, Int. J. Mod. Phys. E 3, 811 (1994).
45 [28] M. El–Nadi, A. Abdelsalam, and N. Ali–Moussa, Radiat. Phys. Chem. 47, 681 (1996).
46 [29] M. El–Nadi, N. Ali–Mossa, and A. Abdelsalam, IL Nuovo Cimento A 110, 1255 (1998).
47 [30] K. Abdel–Waged, J. Phys. G: Nucl. Part. Phys. 25, 1721 (1999).
48 [31] K. Abdel–Waged, Phys. Rev. C 59, 2792 (1999).
49 [32] A. Abdelsalam, B. M. Badawy, and E. El–Falaky, Can. J. Phys. 85, 837 (2007).
50 [33] B. M. Badawy, Int. J. Mod. Phys. E 18, 648 (2009).
51 [34] A. Abdelsalam, B. M. Badawy, and M. Hafiz, Can. J. Phys. 90, 515 (2012).
52 [35] A. Abdelsalam, E. A. Shaat, Z. Abou–Moussa, B. M. Badawy, and Z. S. Mater, Chinese Physics C
53 37, 084001 (2013).
54 [36] B. M. Badawy, Chinese Physics C 38, 114001 (2014).
55 [37] M. I. Adamovich et al for EMU01 Collaboration, Z. Phys. A 358, 337 (1997).
56
57
58
59
60

- 1
2
3
4
5
6 [38] Vladimir Uzhinsky, Joint International Conf. on Supercomputing in Nuclear Applications and Monte
7 Carlo 2010 (SNA+MC 2010), Hitotsubashi Memorial Hall, Tokyo, Japan, October 17 – 21, 2010.
8 “Development of the Fritiof Model in Geant4”.
- 9 [39] K. Abdel-Waged and V. V. Uzhinsky, Phys. Atom. Nucl. 60, 828 (1997); Yad. Fiz. 60, 925 (1997).
10 [40] K. Abdel-Waged and V. V. Uzhinsky, J. Phys. G 24, 1723 (1997).
11 [41] M. El-Nadi, A. Abdel Salam, A. Hussein, E. A. Shaat, N. Ali-Mousa, Z. Abou-Mousa, S. Kamel,
12 Kh. Abdel-Waged and E. El-Falaky, Int. J. Mod. Phys. E 6, 191 (1997).
13 [42] Fu-Hu Liu, Nucl. Phys. A 810, 159 (2008).
14 [43] M. A. Rahim, S. Fakhraddin, and H. Asharabi, Eur. Phys. J. A 48, 115 (2012).
15 [44] Bo Nilsson-Almqvist and Evert Stenlund, Comp. Phys. Comm. 43, 387 (1987).
16 [45] J. Allison et al for GEANT4, Nuclear Instruments and Methods in Physics Research A 835, 186
17 (2016).
18 [46] S. Yu. Shmakov and V. V. Uzhinskii, Com. Phys. Comm., 54, 125 (1989).
19 [47] Fu-Hu Liu and Jun-Sheng Li, Phys. Rev. C 78, 044602 (2008).
20 [48] F. H. Liu, Euro. Phys. Lett. 63, 193 (2003).
21 [49] F. H. Liu, N. N. Abd Allah, D. H. Zhang, and M. Y. Duan, Int. J. Mod. Phys. E 12, 713 (2003).
22 [50] F. H. Liu, N. N. Abd Allah, and B. K. Sing, Phys. Rev. C 69, 057601 (2004).
23 [51] A. Abdelsalam, M. S. El-Nagdy, B. M. Badawy, W. Osman, and M. Fayed, International Journal of
24 Modern Physics E 25, 1650034 (2016).
25 [52] C. F. Powell, F. H. Fowler, and D. H. Perkins, The Study of Elementary Particles by the
26 Photographic Method, Pergamon Press. London, New York, Paris, Los Angeles, 474 (1958).
27 [53] H. Barkas, Nuclear Research Emulsion, Vol. I, Technique and Theory Academic Press Inc., (1963).
28 [54] M. I. Adamovich et al for EMU01 Collaboration, J. Phys. G: Nucl. Part. Phys. 22, 1469 (1996).
29 [55] J. R. Florian, M. Y. Lee, J. J. Lord, J. W. Martin, R. J. Wilkes, R. E. Gibbs, and L. D. Kirkpatrick,
30 Phys. Rev. D 13, 558 (1976).
31 [56] A. Abdelsalam, JINR Report (Dubna), E1-81-623 (1981).
32 [57] Zhang Dong-Hai, Zhao Hui-Hua, Liu Fang, He Chun-Le, Jia Hui-Ming, Li Xue-Qin, Li Zhen-Yu,
33 Li Jun-Sheng, Chinese Physics 15, 1987 (2006).
34 [58] A. Dąbrowska, R. Hołyński, A. Jurak, A. Olszewski, M. Szarska, A. Trzupek, B. Wilczyńska, H.
35 Wilczyński, W. Wolter, B. Wosiek, K. Woźniak, M. L. Cherry, W. V. Jones, K. Sengupta, J. P.
36 Wefel, P. S. Freier, and C. J. Waddington for KLM Collaboration, Phys. Rev. D 47, 1751 (1993).
37 [59] J. J. Lu, D. Beavis, S. Y. Fung, W. Gorn, A. Huie, G. P. Kiernan, R. T. Poe, and G. Van Dalen, Phys.
38 Rev. Lett. 46, 898 (1981).
39
40
41
42
43
44
45
46
47
48
49
50
51
52
53
54
55
56
57
58
59
60